

# Supporting Information

Leroux et al. 10.1073/pnas.0803689105

## SI Text

### Materials and Methods

**Site-Directed Mutagenesis, Protein Production, and Purification.** The *D. fructosovorans* and *E. coli* strains, plasmids and growth conditions used in this study are described in ref. 1.

The Quikchange XL mutagenesis kit (Stratagene) was used to generate point mutations in the large subunit *hynB*. The *AatII-PstI* fragment from pBGF4 was subcloned in pUC18 to generate a template that was used in mutagenesis experiments. After having performed the mutagenesis following the manufacturer's instructions, the *AatII-PstI* fragment was fully sequenced and inserted in the *AatII-PstI* digested pBGF4. The recombinant plasmids were introduced into *D. fructosovorans* strain MR 400 by electrotransformation (2).

The Strep tag II sequence (IBA) was introduced at the 5' terminus of the large subunit gene and the protein was purified using the Strep-Tactin Superflow resin (IBA). MR 400 cells producing WT and variant hydrogenases were harvested, resuspended in Tris/HCl 100 mM pH 8, 150 mM NaCl (buffer A) and disrupted in a French press. After centrifugation at 193000g for 90min, the supernatant was loaded onto a column of Strep-Tactin Superflow resin (1 × 25 cm) equilibrated with buffer A. After washing with buffer A, hydrogenase was eluted with buffer A containing 2.5 mM desthiobiotin. The buffer was exchanged against 50 mM Hepes/NaOH pH 7.5 (buffer B) and the proteins were concentrated to ≈2 ml using a Vivaspin 20 concentrator (30,000 MWCO PES membrane, Vivasciences). An additional anion exchange purification step using a 1 ml HiTrap Q HP column (GE Healthcare) was performed to remove any contaminant. The protein was loaded onto the column equilibrated with buffer B and eluted with a linear gradient of 1M NaCl. The hydrogenase-containing fractions were pooled and the buffer was exchanged against 50 mM Hepes/NaOH, pH 8.

We describe in the main text the properties of the L122F-V74I and L122M-V74M mutants. The four corresponding single mutants were originally purified and tested (i) in solution assays of H<sub>2</sub> oxidation, and (ii) using PFV to determine the  $K_m$  for H<sub>2</sub> and the rates of inhibition. Three of these mutants (L122F, V74I, L122M) displayed the WT phenotype and were not further characterized. The V74M mutant has slightly different properties, which will be reported elsewhere (unpublished work).

**EPR and Potentiometric Titrations.** The EPR spectra were recorded on a Bruker ELEXSYS E500 spectrometer fitted with an Oxford Instruments ESR 900 helium flow cryostat. For spin quantitation, the double integration of the signal recorded under non saturating conditions was compared with that given by a CuSO<sub>4</sub> (1 mM) standard at the same temperature.

The redox titration of the mutants was carried out at 25°C in a specially designed anaerobic cell containing a solution of purified enzyme (≈ 60 μM) in 50 mM Hepes buffer at pH 8 under an atmosphere of Ar. Redox potentials were measured with a combined Pt-Ag/AgCl/KCl (3M) microelectrode, in the presence of a mixture of mediators consisting of 6 μM in each of 1,2 naphthoquinone, resorufine, phenosafranine, neutral red and methyl viologen. The titration was conducted by stepwise additions of small amounts of sodium dithionite solution (10 mM in oxygen-free Hepes buffer). All potentials are quoted against the standard hydrogen electrode (SHE).

**Hydrogen Oxidation Assays.** The assays were carried out as described (4). The purified enzymes were activated for 1h at 37°C in an anaerobic cuvette containing 500 μl of 100 mM Tris/HCl buffer at pH 8 with 2 mM MV. H<sub>2</sub>-oxidation activity was measured at 30°C in a UV cuvette containing 1 ml of buffer Tris/HCl 100 mM at pH 8 with 50 mM methyl viologen (MV, caution: toxic and suspected mutagen). Oxygen was removed under vacuum, the cuvette was flushed with pure H<sub>2</sub>, and dithionite was added to eliminate the residual oxygen. The reaction was started by the addition of 5–20 μl of stock solution of activated enzyme (30–55 nM), and the rate of MV reduction was measured at 604 nm with a UV 1601 spectrophotometer (Shimadzu).

**Isotope-Exchange Assays.** Isotope exchange measurements were carried out using the setup described in ref. 5. D<sub>2</sub> was bubbled in 1.5 ml of 20 mM K-phosphate buffer, pH 7, kept at 30°C in a closed, thermostated vessel. The solution was stirred continuously with a magnetic stirrer. The bottom of the vessel was sealed by a polypropylene membrane, allowing dissolved gases to be directly introduced through a vacuum line into the ion source of the mass spectrometer (model MM 880; VG Instruments). The spectrometer sequentially scans the abundance of the different gases (H<sub>2</sub>, D<sub>2</sub>, HD, and O<sub>2</sub>) by automatically adjusting the magnet current to the corresponding mass peaks ( $m/e = 2, 4, 3,$  and  $32,$  respectively). Measuring one mass peak typically takes 0.5 s. The vessel was closed and anoxia was contained by adding glucose (5 mM), glucose oxidase (30 units), and catalase (500 units). Before measurements, the hydrogenase was activated under an atmosphere of H<sub>2</sub> in the presence of 100 μM reduced methyl viologen. After the enzyme is added, the hydrogenase activity results in D<sup>+</sup>/H<sup>+</sup> scrambling, which is detected by continuously monitoring the consumption of D<sub>2</sub> and the formation of HD and H<sub>2</sub>. The spectrometer sensitivity was calibrated, and the first-order rate constants for gas consumption by the spectrometer were determined in control experiments where the solution was initially saturated under an atmosphere of known composition, and the exponential decrease of the concentration over time was monitored.

**Protein Film Voltammetry.** We used the electrochemical setup and equipment described in ref. 3. All PFV experiments were carried out in a glove box (Jacomex) under a N<sub>2</sub> atmosphere (O<sub>2</sub> < 1 ppm). The electrochemical cell, thermostated at the desired *T* using a water circulation system, was housed in a Faraday cage. A PGE rotating disk working electrode (area  $A \approx 3 \text{ mm}^2$ ) was used in conjunction with an EG&G M636 electrode rotator, a platinum wire was used as a counter electrode, and a saturated calomel electrode (SCE), located in a Luggin side arm containing 0.1 M NaCl and maintained at room temperature, was used as a reference. All potentials are quoted versus the standard hydrogen electrode (SHE),  $E_{\text{SHE}} = E_{\text{SCE}} + 241 \text{ mV}$  at room temperature.

The mixed buffer consisted of Mes, Hepes, sodium acetate, TAPS, and CHES (5 mM of each component), 1 mM EDTA, and 0.1 M NaCl as supporting electrolyte.

Before preparing an enzyme film, the PGE electrode was polished with an aqueous alumina slurry (Buehler, 1  $\mu\text{m}$ ) and sonicated thoroughly. Protein films were prepared by painting the electrode with about half a microliter of a stock solution of enzyme ( $\approx 0.4\text{mg/ml}$  in the mixed buffer at pH 7). To activate the enzyme, the enzyme-coated electrode was inserted in the electrochemical cell containing the buffer at pH 4, 40°C, under an atmosphere of  $\text{H}_2$ , and poised at  $-560\text{mV}$  vs. SHE for  $\approx 1$  hour. The extent of activation was monitored by taking the electrode potential to  $-160\text{mV}$  to measure the  $\text{H}_2$  oxidation current. The electrode could then be rinsed and transferred to a fresh solution with very little loss in electroactive coverage over time.

For measuring the Michaelis constant for  $\text{H}_2$ , we used a modified version of the method exposed in ref. 3, which we described in ref. 6. (Figure 24, section 2.4.2 therein). The electrochemical cell was flushed with  $\text{H}_2$  (from Air Liquide) using a cannula to bubble the gas directly into the cell solution. While the activity was measured at  $-160\text{mV}$ , pH 7, at a certain  $T$  in the range 5–40°C,  $\text{H}_2$  initially dissolved in concentration  $[\text{H}_2]_0$  was flushed away by bubbling argon in the cell at  $t \geq t_0$ . The time-dependent substrate concentration is  $[\text{H}_2] = [\text{H}_2]_0 \exp[-(t-t_0)/\tau]$ . Because Michaelis–Menten kinetics is obeyed (3), the activity evolves with time according to

$$i(t) = \frac{i^{\max}}{1 + \frac{K_m}{[\text{H}_2]_0} \exp \frac{t - t_0}{\tau}}$$

where  $i^{\max}$  is the current extrapolated to infinite concentration of substrate. If  $K_m/[\text{H}_2]_0$  is small enough, the change in activity against time is a portion of a sigmoid and the value of  $K_m/[\text{H}_2]_0$  can be determined by fitting the data. Hence the  $K_m$  value is obtained as a fraction of the concentration of  $\text{H}_2$  that is dissolved at the temperature where the experiment is carried out.

For determining the kinetics of CO binding and release (experiments in Fig. 3), the electrochemical cell was continuously flushed with  $\text{H}_2$ . The same buffer as that present in the electrochemical cell, but saturated with CO at 25°C (with the safety precautions relevant to the high toxicity of carbon monoxide) was kept in a capped serum bottle. Small aliquots of this solution were injected into the electrochemical cell using gas-tight syringes. In the caption of Fig. 3, consistently with refs. 3 and 7, we note  $x$  the volumic fractions that refer to the amount of solution injected:  $x$  is the volume injected divided by total volume of solution in the cell after the injection; it is also the ratio of the concentration of gas at time of injection over the concentration under saturating conditions at 25°C,  $x = C(t = 0)/C(\text{sat})$ . Hence “one atm of CO” in Table 1 refers to the concentration of CO in a solution that is equilibrated with pure CO at 25°C. In the experiments in Fig. 3, the concentration of CO changes against time,  $[\text{CO}] = [\text{CO}]_0 \exp(-t/\tau)$ , but the value of  $[\text{CO}]_0$  is independent of the temperature of the buffer in the electrochemical cell (it only depends on how much solution saturated under 1 atm CO at 25°C is injected). The value of  $\tau$  depends on  $T$  and on other experimental parameters, but it is independently determined from fitting the data.

We analyzed the electrochemical data using “SOAS,” an in-house program available on our web site at <http://bip.cnrs-mrs.fr/bip06/software.html>.

### Kinetic Models and Data Analysis

**CO Inhibition.** We recall here the method described in refs. 6 and 7. We assume that the active form of the enzyme converts to a CO-bound, inhibited form with a pseudo first-order rate constant that depends on the instant concentration of CO. CO is flushed away from the cell by bubbling hydrogen directly into the cell solution so that both the CO concentration and the rate of inactivation decrease exponentially with time. If we call  $k_{\text{in}}^{\text{CO}}[\text{CO}]_0$  the initial rate of inactivation, just after CO is added, then the time-dependent rate of inactivation is  $k_{\text{in}}^{\text{CO}}[\text{CO}]_0 \exp(-t/\tau)$ . The first-order rate of activation is  $k_{\text{out}}^{\text{CO}}$ .



We call  $y(t)$  the fraction of enzyme in the active (CO-free) state, and  $1 - y(t)$  the fraction of enzyme inhibited by CO.  $y(t)$  obeys the following differential equation:

$$dy/dt = -k_{\text{in}}^{\text{CO}}[\text{CO}]_0 e^{-t/\tau} y + k_{\text{out}}^{\text{CO}}(1 - y) \quad [2]$$

with the initial condition  $y(0) = 1$  (the enzyme is fully active before CO is injected).

The solution gives the evolution of the relative activity  $y(t)$  as a function of the parameters  $k_{\text{in}}^{\text{CO}}[\text{CO}]_0$ ,  $k_{\text{out}}^{\text{CO}}$ ,  $\tau$ :

$$y(t) = e^{k_{\text{in}}^{\text{CO}}[\text{CO}]_0 \tau e^{-\frac{t}{\tau}} - k_{\text{out}}^{\text{CO}} t} \times \left( e^{-k_{\text{in}}^{\text{CO}}[\text{CO}]_0 \tau} + \int_0^t k_{\text{out}}^{\text{CO}} e^{-k_{\text{in}}^{\text{CO}}[\text{CO}]_0 \tau e^{-\frac{u}{\tau}} + k_{\text{out}}^{\text{CO}} u} du \right) \quad [3]$$

This was used to fit the change in current in Fig. 3 to determine  $k_{\text{out}}^{\text{CO}}$  and  $k_{\text{in}}^{\text{CO}}[\text{CO}]_0$ , as described in ref. 7. We found that the adjusted value of  $k_{\text{in}}^{\text{CO}}[\text{CO}]_0$  was proportional to the amount of CO that is injected at  $t = 0$ ; this confirmed the hypothesis of bimolecular inhibition kinetics.

**Isotope-exchange.** We interpret the isotope exchange kinetics using the analytical solution of the reaction scheme in Fig. S1. We note  $[\text{D}_2]$ ,  $[\text{HD}]$  and  $[\text{H}_2]$  the concentrations of dissolved gases;  $c_0$  is the initial concentration of  $\text{D}_2$  ( $c_0 = [\text{H}_2] + [\text{HD}] + [\text{D}_2]$ ). We note  $[\text{ee}]$ ,  $[\text{dd}]$ ,  $[\text{dh}]$ ,  $[\text{hh}]$  the concentrations of enzymes that are either free or bound to DD, DH, and HH, respectively. We assume that the states  $hd$  and  $dh$  interconvert rapidly (this involves the dissociation and primary geminate recombination of HD).  $e_0 = [\text{ee}] + [\text{dd}] + [\text{dh}] + [\text{hh}]$  is the total concentration of enzyme ( $e_0 \ll c_0$ ).

In Fig. S1,  $k_{\text{out}}$  is the first-order rate constant which incorporates gas dissociation and diffusion to the bulk,  $k_{\text{in}}$  is the bimolecular rate constant which relates to gas diffusion toward the active site and binding,  $k$  is the rate of  $\text{H}^+/\text{D}^+$  exchange. The rate constant from  $dh$  to  $hh$  is  $k/2$  (rather than  $k$ ) because we assume that the forms  $dh$  and  $hd$  are in rapid equilibrium, but only one of them has the  $\text{D}^+$  on the active site base, ready to be exchanged.

The differential equations that describe the evolution of the system are:

$$d[ee]/dt = -k_{\text{in}} \times [ee] \times ([\text{D}_2] + [\text{HD}] + [\text{H}_2]) + k_{\text{out}}([hh] + [dh] + [dd]) \quad [4a]$$

$$d[dd]/dt = k_{\text{in}} \times [ee] \times [\text{D}_2] - (k + k_{\text{out}}) \times [dd] \quad [4b]$$

$$d[dh]/dt = k_{\text{in}} \times [ee] \times [\text{HD}] + k \times [dd] - (k_{\text{out}} + k/2) \times [dh] \quad [4c]$$

$$d[hh]/dt = k_{\text{in}} \times [ee] \times [\text{H}_2] + k/2 \times [dh] - k_{\text{out}} \times [hh] \quad [4d]$$

$$d[\text{D}_2]/dt = -k_{\text{in}} \times [\text{D}_2] \times [ee] + k_{\text{out}} \times [dd] \quad [4e]$$

$$d[\text{HD}]/dt = -k_{\text{in}} \times [\text{HD}] \times [ee] + k_{\text{out}} \times [dh] \quad [4f]$$

$$d[\text{H}_2]/dt = -k_{\text{in}} \times [\text{H}_2] \times [ee] + k_{\text{out}} \times [hh] \quad [4g]$$

and the initial conditions are  $[ee] = e_0$ ,  $[dd] = 0$ ,  $[dh] = 0$ ,  $[hh] = 0$ ,  $[\text{D}_2] = c_0$ ,  $[\text{HD}] = 0$ ,  $[\text{H}_2] = 0$ . The steady state values of  $[ee]$ ,  $[dd]$ ,  $[hh]$  are obtained by solving

$$\begin{pmatrix} d[ee]/dt \\ d[dd]/dt \\ d[dh]/dt \\ e_0 \end{pmatrix} = \begin{pmatrix} -k_{\text{in}}([\text{D}_2] + [\text{HD}] + [\text{H}_2]) & k_{\text{out}} & k_{\text{out}} & k_{\text{out}} \\ k_{\text{in}} \times [\text{D}_2] & -k - k_{\text{out}} & 0 & 0 \\ k_{\text{in}} \times [\text{HD}] & k & -k_{\text{out}} - k/2 & 0 \\ 1 & 1 & 1 & 1 \end{pmatrix} \begin{pmatrix} [ee] \\ [dd] \\ [dh] \\ [hh] \end{pmatrix} = \begin{pmatrix} 0 \\ 0 \\ 0 \\ e_0 \end{pmatrix} \quad [5]$$

The result is:

$$[ee] = \frac{e_0}{1 + k'_{\text{in}}c_0} \quad [6a]$$

$$[dd] = \frac{k'_{\text{in}}e_0}{(1 + k'_{\text{in}}c_0)} \frac{[\text{D}_2]}{(1 + k')} \quad [6b]$$

$$[dh] = \frac{k'_{\text{in}}e_0}{(1 + k'_{\text{in}}c_0)} \frac{2(k'[\text{D}_2] + (k' + 1)[\text{HD}])}{(2 + k')(1 + k')} \quad [6c]$$

$$[hh] = \frac{k'_{\text{in}}e_0}{(1 + k'_{\text{in}}c_0)} \frac{(k'^2[\text{D}_2] + k'(k' + 1)[\text{HD}] + (2 + k')(1 + k')[\text{H}_2])}{(2 + k')(1 + k')} \quad [6d]$$

$$k' = k/k_{\text{out}} \quad [6e]$$

$$k'_{\text{in}} = k_{\text{in}}/k_{\text{out}} \quad [6f]$$

This is substituted in Eqs. 4e–4g to obtain the change in gas concentrations against time.

$$[\text{D}_2](t) = c_0 e^{-k_{\text{D}}t} \quad [7a]$$

$$[\text{HD}](t) = 2c_0[e^{-k_{\text{T}}t} - e^{-k_{\text{D}}t}] \quad [7b]$$

$$[\text{D}_2](t) + \frac{[\text{HD}](t)}{2} = c_0 e^{-k_{\text{T}}t} \quad [7c]$$

$$k_{\text{D}} = k_{\text{out}} \frac{k'}{(1 + k')} \frac{k'_{\text{in}}e_0}{(1 + k'_{\text{in}}c_0)} \quad [7d]$$

$$k_{\text{T}} = k_{\text{out}} \frac{k'}{(2 + k')} \frac{k'_{\text{in}}e_0}{(1 + k'_{\text{in}}c_0)} \quad [7e]$$

Eq. 7b shows that  $[\text{HD}]$  reaches a maximum at

$$t_{\text{max}} = \frac{\ln(k_{\text{D}}/k_{\text{T}})}{k_{\text{D}} - k_{\text{T}}} \quad [8]$$

Substituting  $t_{\text{max}}$  into Eq. 4f and letting  $d[\text{HD}]/dt = 0$  gives directly the maximum value of  $[\text{HD}]$ , which depends only on the ratio  $k' = k/k_{\text{out}}$ .

$$\frac{[\text{HD}]_{\text{max}}}{c_0} = \frac{2}{1+k'} \left( \frac{1+k'}{2+k'} \right)^{2+k'} \quad [9]$$

Eq. 9 is plotted in Fig. S2. This working curve makes it possible to estimate  $k/k_{\text{out}}$  from the maximal value of [HD]. This simple model predicts that the concentration of  $\text{D}_2$  and the isotopic content  $T = ([\text{D}_2] + [\text{HD}])/2$  decrease exponentially against time, as indeed observed in experiments, with rate constants  $k_{\text{D}}$  and  $k_{\text{T}}$ , respectively (Eqs. 7a and 7c). The value of  $k'$  can also be determined by combining these rate constants:

$$k' = \frac{2k_{\text{T}} - k_{\text{D}}}{k_{\text{D}} - k_{\text{T}}} \quad [10]$$

In experiments, we observed a background decrease in dihydrogen concentrations resulting from the slow gas consumption by the mass spectrometer. In control experiments carried out in the absence of enzyme, we found that this “leak” occurs with first-order kinetics and rate constants  $k_{\text{leak}}^{\text{H}_2} = 0.095 \text{ min}^{-1}$ ,  $k_{\text{leak}}^{\text{HD}} = 0.089 \text{ min}^{-1}$  and  $k_{\text{leak}}^{\text{D}_2} = 0.083 \text{ min}^{-1}$  (5, 8). This is slow with respect to the isotope exchange catalyzed by the WT enzyme under typical experimental conditions (e.g.,  $k_{\text{D}} = 2 \text{ min}^{-1}$  in the case of the data in Fig. 5), but this is significant in the case of the MM mutant that has slow exchange activity ( $k_{\text{D}} = 0.16 \text{ min}^{-1}$  for the data in Fig. 5). Since the above model does not explicitly include the leak, we proceeded to the following verifications. Concentration changes (as in Fig. 5) were simulated by using a version of Eq. 4 that was modified to take into account the leak (by introducing the last terms in the right-hand sides of Eqs. 11e–11g)

$$d[ee]/dt = -k_{\text{in}} \times [ee] \times ([\text{D}_2] + [\text{HD}] + [\text{H}_2]) + k_{\text{out}}([hh] + [dh] + [dd]) \quad [11a]$$

$$d[dd]/dt = k_{\text{in}} \times [ee] \times [\text{D}_2] - (k + k_{\text{out}}) \times [dd] \quad [11b]$$

$$d[dh]/dt = k_{\text{in}} \times [ee] \times [\text{HD}] + k \times [dd] - (k_{\text{out}} + k/2) \times [dh] \quad [11c]$$

$$d[hh]/dt = k_{\text{in}} \times [ee] \times [\text{H}_2] + k/2 \times [dh] - k_{\text{out}} \times [hh] \quad [11d]$$

$$d[\text{D}_2]/dt = -k_{\text{in}} \times [\text{D}_2] \times [ee] + k_{\text{out}} \times [dd] - k_{\text{leak}}^{\text{D}_2} \times [\text{D}_2] \quad [11e]$$

$$d[\text{HD}]/dt = -k_{\text{in}} \times [\text{HD}] \times [ee] + k_{\text{out}} \times [dh] - k_{\text{leak}}^{\text{HD}} \times [\text{HD}] \quad [11f]$$

$$d[\text{H}_2]/dt = -k_{\text{in}} \times [\text{H}_2] \times [ee] + k_{\text{out}} \times [hh] - k_{\text{leak}}^{\text{H}_2} \times [\text{H}_2] \quad [11g]$$

First, using a Runge-Kutta integrator, we solved this set of equations for reasonable values of the parameters. In a second step, the simulations were analyzed as if they were real data, to deduce  $k/k_{\text{out}}$  using either of the following methods:

1. Using either Eq. 9 or Eq. 10 with no correction.
2. Since the measured  $[\text{HD}]_{\text{max}}/c_0$  is lower than that which would be observed in the absence of leak, the value of  $k'$  deduced from Eq. 9 is overestimated. This can be empirically corrected by replacing  $c_0$  in Eq. 9 with the concentration  $c_0' = ([\text{H}_2] + [\text{HD}] + [\text{D}_2])$  measured at the time [HD] reaches its maximum (Eq. 8), rather than at the time of injection of the enzyme ( $c_0' < c_0$ ).
3. First, correcting the concentration profiles for the leak using the known values of  $k_{\text{leak}}$  and the method described in ref. 5. Then using Eq. 10.

We compared the values of  $k/k_{\text{out}}$  deduced using these methods with those input in the calculations. The corrections provided by methods 2 and 3 improved the estimation given by method 1, except when the exchange activity was at least an order of magnitude faster than the leak (in which case method 1 needs no correction to give an accurate result). In the worst situation (lowest activity),  $k/k_{\text{out}}$  was underestimated by a factor of two by method 2, whereas method 3 consistently provided good estimates. We applied method 1 to calculate the value in Table 1 for the WT enzyme. We used method 3 for both mutants.

1. Dementin S, et al. (2004) A glutamate is the essential proton transfer gate during the catalytic cycle of the NiFe hydrogenase. *J Biol Chem* 279:10508–10513.
2. Rousset M, et al. (1998) New shuttle vectors for the introduction of cloned DNA in *Desulfovibrio*. *Plasmid* 39:114–122.
3. Léger C, et al. (2004) Inhibition and aerobic inactivation kinetics of *Desulfovibrio fructosovorans* NiFe hydrogenase studied by protein film voltammetry. *J Am Chem Soc* 126:12162–12172.
4. Dementin S, et al. (2006) Changing the ligation of the distal [4Fe4S] cluster in NiFe hydrogenase impairs inter- and intramolecular electron transfers. *J Am Chem Soc* 128:5209–5218.
5. Cournac L, Guedeney L, Peltier G, Vignais PM (2004) Sustained photoevolution of molecular hydrogen in a mutant of *Synechocystis* sp. strain PCC 6803 deficient in the type I NADPH-dehydrogenase complex. *J Bacteriol* 186:1737–1746.
6. Léger C, Bertrand P (2008) Direct electrochemistry of redox enzymes as a tool for mechanistic studies *Chem. Rev* 108:2379–2438.
7. Almeida MG, et al. (2007) A needle in a haystack: the active site of the membrane-bound complex cytochrome *c* nitrite reductase. *FEBS Letts* 581:284–288.
8. Jouanneau Y, et al. (1980) Continuous monitoring, by mass spectrometry, of  $\text{H}_2$  production and recycling in *Rhodospseudomonas capsulata*. *J Bacteriol* 143:628–636.

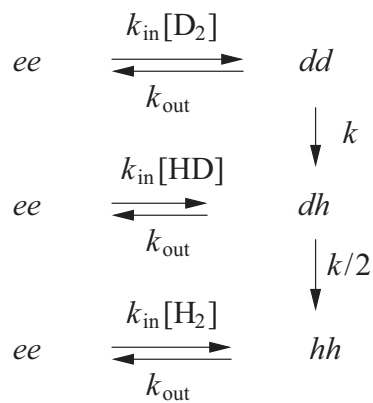


**Fig. S1.** Simplified scheme used for relating the kinetics of isotope exchange to the rates of intramolecular diffusion. *ee*, *dd*, *dh*, *hh* depict the enzyme that is either free or bound to DD, DH, and HH, respectively.

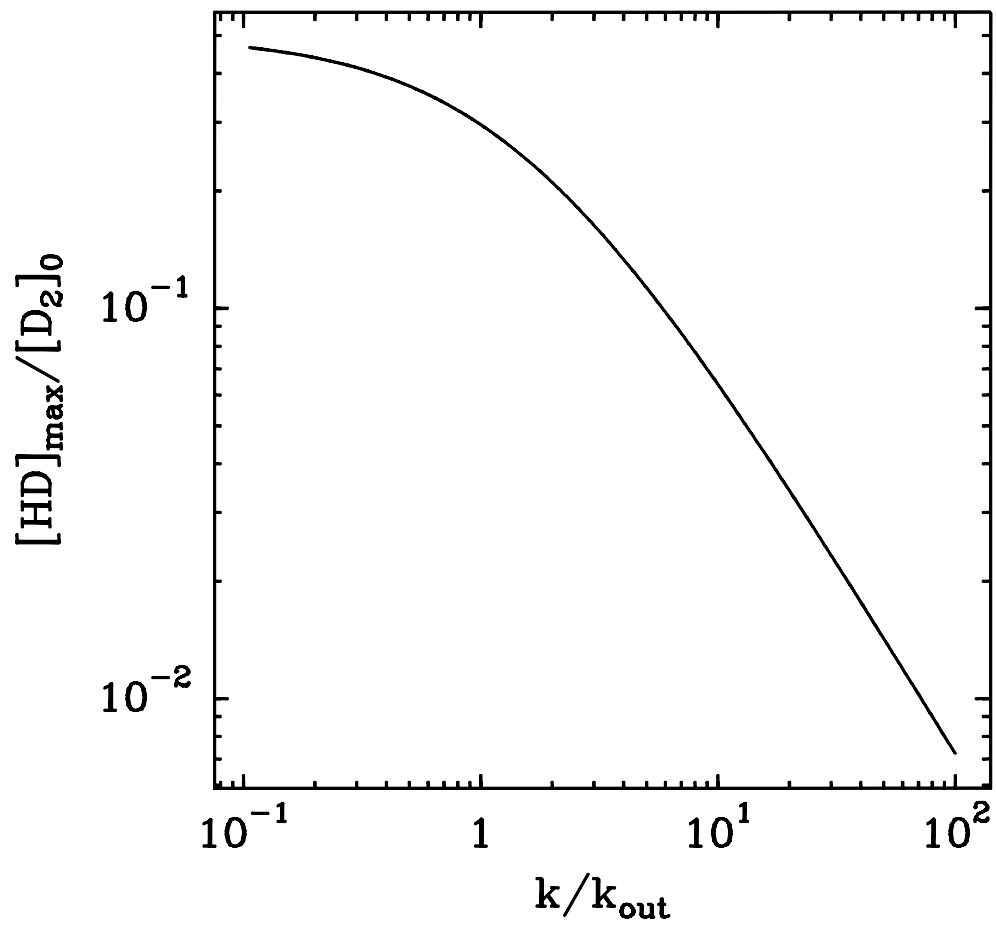
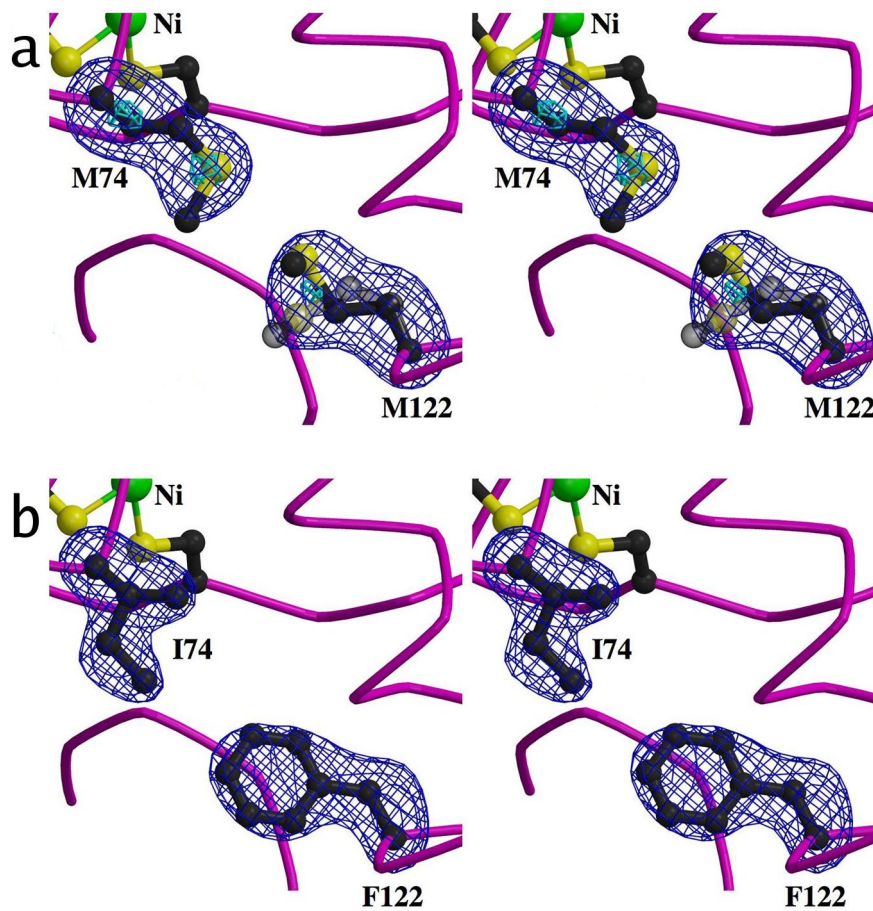


Fig. S2. Maximal concentration of HD, normalized to the initial concentration of  $D_2$ , as a function of the dimensionless parameter  $k' = k/k_{out}$ , according to Eq. 9.



**Fig. S3.** Electron density maps. Stereo image of a 3-fold averaged omit  $mF_o - F_c$  electron density map of the side-chains of the mutated residues for the MM (a) mutant and FI mutant (b). Used contour levels 4  $\sigma$  (dark-blue) and 12  $\sigma$  (light-blue), 1  $\sigma$  being the rms. level of the respective maps.

**Table S1. Characteristics of the EPR signatures of the three enzymes in the oxidized states**

Variant	Species	$g_x$	$g_y$	$g_z$
WT	Ni-A	2.314	2.232	2.01
WT	Ni-B	2.338	2.157	2.01
FI	Ni-A	2.311	2.231	2.005
MM	Ni-A	2.307	2.226	2.005
MM	Ni-B	2.330	2.154	2.005

Table S2. X-ray data statistics

	MM	FI
X-ray wavelength, Å	1.0	0.934
Space group	P2 <sub>1</sub>	P2 <sub>1</sub>
Cell dimensions: $\beta$ , °	91.6	92.2
a, b, c, Å	64.6, 99.9, 183.0	62.3, 99.6, 182.2
Molecules/asymmetric unit	3	3
Resolution, Å*	25–2.4 (2.5–2.4)	20–2.18 (2.3–2.18)
$R_{\text{sym}}$ , %*	9.5 (24.0)	7.0 (19.8)
$\langle I \rangle / \langle \sigma(I) \rangle$ *	11.8 (4.4)	7.2 (3.3)
Unique reflections*	86780 (8361)	108157 (14513)
Completeness, %*	95.3 (80.1)	93.3 (84.6)
Redundancy*	4.6 (2.3)	2.6 (2.2)

\*Numbers in parentheses refer to the highest-resolution shell.

**Table S3. Crystallographic refinement statistics**

	MM	FI
Resolution, Å	25–2.4	20–2.2
Reflections in work set	82430	101754
$R_{\text{work}}$ , %	14.9	18.5
Reflections in test set	4350	5404
$R_{\text{free}}$ , %	19.3	22.2
Total number of atoms	19506	19605
Water molecules	867	1019
$\sigma_{\text{bond}}$ , Å	0.010	0.012
$\sigma_{\text{angle}}$ , °	1.21	1.27
Average B factors, Å <sup>2</sup>		
Molecule 1	35.5	10.6
Molecule 2	46.0	20.8
Molecule 3	41.6	15.7